arXiv:2611.09864v1 [cs.RO] 6 Nov 2026

Grasp-TAGS: Task-Aware Grasp Selection via Critic Distillation for Prehensile Loco-Manipulation

Xun Tu, Minghao Zou, and Karthik Desingh

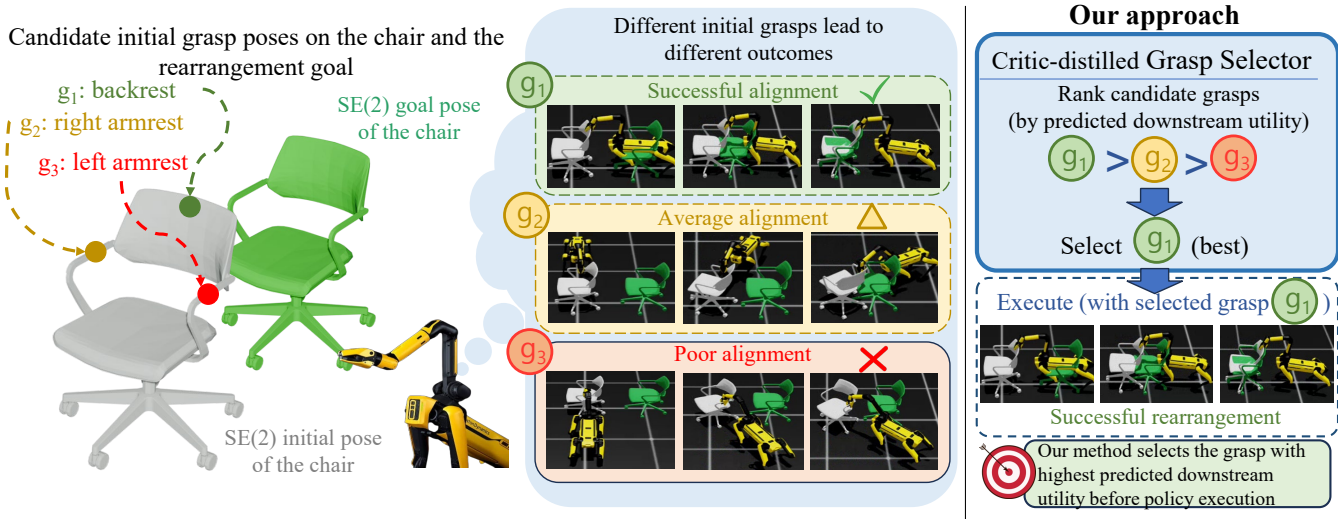


Fig. 1: **Overview of the Grasp-TAGS framework.** Different feasible grasp poses on the same object can induce substantially different downstream loco-manipulation behaviors and rearrangement outcomes. For example, three grasp poses g_1, g_2, and g_3 on the chair shown here can have different behaviors for moving the chair from its initial pose to the final pose. At inference time, our critic-distilled grasp selector ranks candidate grasps by their predicted downstream task utility, selects the highest-utility grasp for the desired object pose, and executes the manipulation policy from the selected grasp configuration.

***Abstract*— Loco-manipulation, which requires mobile manipulators to coordinate locomotion and manipulation over long horizons, is a key capability for large-object rearrangement in applications such as service robotics and warehouse automation. Despite recent progress, reliably executing these tasks remains challenging because performance depends on complex robot-object and object-environment interaction dynamics. Existing approaches address this challenge either through model-based methods, which often require accurate dynamics models, or through learning-based methods, which reduce this requirement but typically assume a fixed or predefined initial grasp. However, different geometrically stable grasps can lead to substantially different downstream manipulation performance. Therefore, we propose Grasp-TAGS, a task-aware grasp selection framework for goal-conditioned large-object rearrangement. We train a unified PPO-based reinforcement learning policy across multiple initial grasp configurations and distill the learned critic into a lightweight grasp utility network that ranks candidate grasps using only the candidate grasp configuration and goal information. At inference time, we select the grasp with the highest predicted downstream utility for the downstream policy to complete the task, before even making a contact. Experiments demonstrate that Grasp-TAGS improves rearrangement success over both fixed single-grasp policies and random grasp selection, achieving an average success rate of 89.84% compared with 79.87% for the best-performing single-grasp policies, an improvement of 9.97 percentage points. Grasp-TAGS also reduces final orientation errors across all evaluated objects. For more qualitative results, refer to the supplementary webpage: `https://rpm-lab-umn.github.io/Grasp-TAGS-web-page/`.**

All authors are affiliated with the Department of Computer Science & Engineering at the University of Minnesota, Twin Cities. Contact:{tu000080, zou00189, kdesingh}@umn.edu

I. Introduction

Loco-manipulation enables a mobile robot to coordinate base locomotion and manipulation to physically interact with objects over extended horizons and accomplish manipulation tasks. Large-object rearrangement is a particularly challenging instance of loco-manipulation, where bulky or heavy objects such as chairs, carts, and luggage must be transported to desired poses [1]–[4]. Because such objects are often impractical to lift, the robot must manipulate them while they remain in contact with the ground, resulting in complex physical interactions not only between the robot and object, but also between the object and its surroundings. Managing these coupled interactions throughout the rearrangement process requires sustained contact, coordinated base-arm motion, and robust control throughout prolonged robot-object-environment interaction. Addressing these challenges is therefore critical to enabling reliable loco-manipulation in real-world applications such as warehouse automation, service robotics, and assistive robotics.

Prior work has addressed loco-manipulation skills for large-object rearrangement using model-based approaches such as model predictive control (MPC), which explicitly model system dynamics and generate whole-body motions through analytical planning and control [5], [6]. These approaches generally rely on sufficiently accurate knowledge

of the underlying dynamics. More recently, learning-based methods using reinforcement learning and imitation learning have demonstrated promising performance [4], [7]–[9]. By learning control policies from simulated interactions or demonstrations, these methods reduce the need to explicitly model complex robot-object-environment dynamics during execution. However, existing learning-based approaches typically assume a fixed or predefined initial grasp configuration before downstream manipulation.

This assumption is restrictive, as the initial grasp choice can substantially influence subsequent rearrangement. The initial grasp affects downstream rearrangement by changing contact locations and the corresponding arm configuration. These differences alter the motions and forces the robot can effectively apply during pushing or dragging, which in turn influence object controllability and task outcome, as illustrated in Fig. 2.

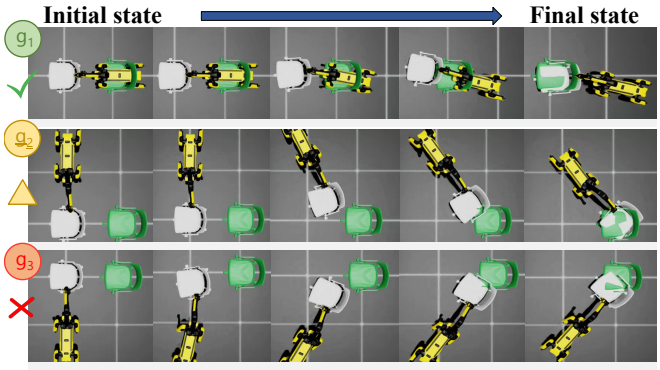


Fig. 2: **Qualitative example of grasp-dependent rearrangement behavior.** For the illustrated target pose, the backrest grasp (g_1) yields better final alignment with the target pose than the two armrest grasps (g_2 and g_3).

Consequently, even among geometrically feasible and physically stable grasps, downstream performance can vary substantially with the rearrangement goal. We therefore hypothesize that, for large-object rearrangement, the initial grasp should be treated as a task-dependent decision variable rather than a fixed or random configuration. Specifically, selecting the grasp with the highest expected downstream task utility from multiple feasible candidates should improve rearrangement performance compared with fixed or random grasp selection.

To this end, we propose Grasp-TAGS, a Task-Aware Grasp Selection framework for goal-conditioned large-object rearrangement, as illustrated in Fig. 1. Grasp-TAGS evaluates candidate grasps according to their expected downstream task utility and selects the most suitable grasp before manipulation begins. We first train a unified manipulation policy via PPO across multiple feasible initial grasp configurations, allowing both the policy and its critic to capture grasp-dependent downstream behavior. Consequently, the critic assigns different value estimates to initial states associated with different candidate grasps. We then distill these grasp-dependent values into a lightweight grasp utility network using only information available prior to physical interaction. At inference time, the network ranks candidate grasps for the specified rearrangement goal, selects the grasp with the highest predicted utility, and executes the unified manipulation policy from the selected configuration. We evaluate the proposed framework on goal-conditioned rearrangement of multiple large household objects in simulation to validate the pipeline's effectiveness in selecting the high-utility grasp configuration for large-object rearrangement.

In summary, our contributions are:

- We present a unified goal- and grasp-conditioned loco-manipulation policy trained via PPO that operates across multiple initial grasp configurations for large-object rearrangement.
- We propose a critic-distillation method where the critic is distilled into a lightweight grasp utility network that predicts downstream grasp utility from pre-interaction grasp and goal information, enabling task-aware grasp selection at inference time.
- We show that different feasible grasps can lead to substantially different downstream manipulation outcomes, and that our proposed grasp selection framework, Grasp-TAGS, improves task success over fixed or random grasp selection, through simulation experiments

II. Related Work

A. Large Object Rearrangement in Loco-Manipulation

Large-object rearrangement remains a challenging problem in Loco-manipulation. In this work, we refer to large objects as bulky objects that extend beyond the conventional tabletop manipulation setting, such as chairs and carts [1]. Their size and weight require robots to coordinate base locomotion and end-effector motion to push or pull while firmly holding the object toward a desired pose [2]–[4].

Early approaches primarily relied on model-based methods, such as model-predictive control (MPC), to explicitly account for object dynamics and execute whole-body motions analytically in accordance with dynamical laws in physics [5], [6], [10]–[12]. More recently, data-driven approaches based on reinforcement learning (RL) and imitation learning (IL) have emerged as an alternative to directly handling the complex interaction dynamics of large-object manipulation by learning the knowledge of interaction [3], [4], [7]–[9], [13]–[15]. For instance, Ravan et al. [8] develop a teleoperation-based pipeline to collect demonstrations of a quadrupedal robot and subsequently train a diffusion policy [16]. In contrast, ALORE [7], RobotMover [4], and ReLIC [9] adopt hierarchical reinforcement learning to learn manipulation policies in simulation and transfer them to real-world platforms. Such approaches reduce the reliance on costly expert demonstrations and enable scalable policy learning through simulation.

Despite these advances, existing learning-based approaches typically assume a single predefined initial grasp pose (with positional variance smaller than 10 cm) [3], [4], [7], [8]. This assumption overlooks that larger-scale grasp configurations (positional variance larger than 30 cm) can induce substantially different interaction dynamics, leading

to different downstream manipulation performance. Some prior works relax the assumption of a fixed interaction configuration in non-prehensile manipulation. Polverini et al. [17] exploit multiple robot–environment contacts to push a heavy object, while Dadiotis et al. [12] learn to adapt the pushing location and direction when transporting unknown objects toward target poses. However, these works focus on non-prehensile pushing, where contact locations can be adjusted during execution. In contrast, we consider prehensile large-object rearrangement, where the robot must select among spatially distinct candidate grasps on different object parts before manipulation begins and maintain the selected grasp throughout the task.

B. Grasp Planning and Task-Oriented Grasp Selection

Grasp planning aims to identify end-effector poses that establish stable contact with a target object [1]. Given that multiple feasible grasps may exist, grasp pose evaluation and selection determine which candidate to execute. Prior approaches mainly evaluate grasps using analytical criteria such as contact forces, object stability, and wrench-based measures [1], [18]–[20]. More recent learning-based methods estimate grasp quality directly from visual observations or point clouds [21]–[23] using expert datasets.

These approaches primarily assess grasp feasibility and stability, without considering their impact on downstream manipulation. Recent task-oriented grasping methods address this limitation by selecting grasps according to the intended manipulation objective [24]–[28]. However, these methods predominantly focus on tabletop manipulation, where tasks are relatively short-horizon, and objects are typically smaller and lighter. In contrast, large-object rearrangement requires long-horizon loco-manipulation, where different grasp locations can induce substantially different robot-object configurations and consequently affect downstream task execution [1], [8]. In this work, we study task-aware grasp selection for goal-conditioned large-object rearrangement by ranking feasible candidate grasps according to their expected downstream task utility rather than grasp feasibility alone.

C. Conditioned Policy Learning

Conditioned policy learning incorporates task-level or contextual variables into policy learning, enabling a single policy to adapt its behavior to different task objectives and environments. In imitation learning, policies have been conditioned on variables such as target object poses [16], [29], [30], language instructions [31]–[34], and task parameters [35]. Reinforcement learning similarly enables policies to condition on task parameters [4], [7], [36], object physical attributes [37], and language instructions [38]–[41], allowing agents to acquire diverse behaviors through self-exploration rather than expert demonstrations [42]–[46].

Despite the success of conditioned policy learning, initial grasp pose has received limited attention as a conditioning variable for large-object loco-manipulation. A few recent works incorporate grasp pose into imitation-learning-based policies [47]–[50], but rely on expert demonstrations to learn the corresponding manipulation behaviors. The work most closely related to ours [28] incorporates grasp information into value-based grasp evaluation, but focuses on small, geometrically simple objects in tabletop settings. In contrast, we explicitly condition an RL-based loco-manipulation policy on the initial grasp pose, enabling the policy and its value function (i.e., the critic) to capture the distinct interaction dynamics induced by different grasp configurations. We then distill the learned grasp-dependent value estimates into a grasp-selection network that predicts the expected downstream task utility of candidate grasps before executing the policy.

III. Problem Statement

We consider goal-conditioned large-object rearrangement, where a mobile manipulator moves a target object from an initial pose p_0 to a desired planar pose $p_{goal} = (x, y, \theta) \in SE(2)$. We assume a set of feasible initial grasp poses $g_1, g_2, \cdots, g_K$, each specifying a desired end-effector pose expressed in the target object's local coordinate frame:

$$\mathcal{G} = \{g_1, g_2, \ldots, g_K\} \subset SE(3) \tag{1}$$

Our objective is twofold. First, we learn a manipulation policy $\pi(a_t|o_t, g_i)$ capable of executing the rearrangement task under different $g_i \in \mathcal{G}$. Second, we select the grasp providing the highest expected downstream task utility:

$$g^* = \arg\max_{g_i \in \mathcal{G}} U(g_i, p_{goal}^{obj}), \tag{2}$$

where $U(\cdot)$ represents the expected downstream utility of the candidate grasp g_i with respect to the task objective p_{goal}^{obj}, which is the target pose represented in the initial object frame. The selected grasp g^* is used for downstream manipulation at inference time:

$$a_t \sim \pi(\cdot|o_t, g^*) \tag{3}$$

IV. Methodology

Unlike conventional mobile manipulation settings that assume a fixed grasp configuration, we consider multiple feasible grasp poses on the target object. Each grasp pose induces a distinct robot–object interaction configuration and, consequently, different manipulation dynamics. Our objective is two-fold: (1) learn a unified manipulation policy capable of transporting the object to a desired pose under different grasp configurations, and (2) select, at inference time, the grasp pose with the highest expected utility for successfully completing the rearrangement task (see Fig. 3).

A. Hierarchical Policy Learning

Large-object rearrangement requires coordinated locomotion and manipulation over long horizons [2]. Directly learning a unified whole-body policy over all robot joints is challenging due to the high-dimensional action space and complex robot-object interactions [4], [7]. To improve

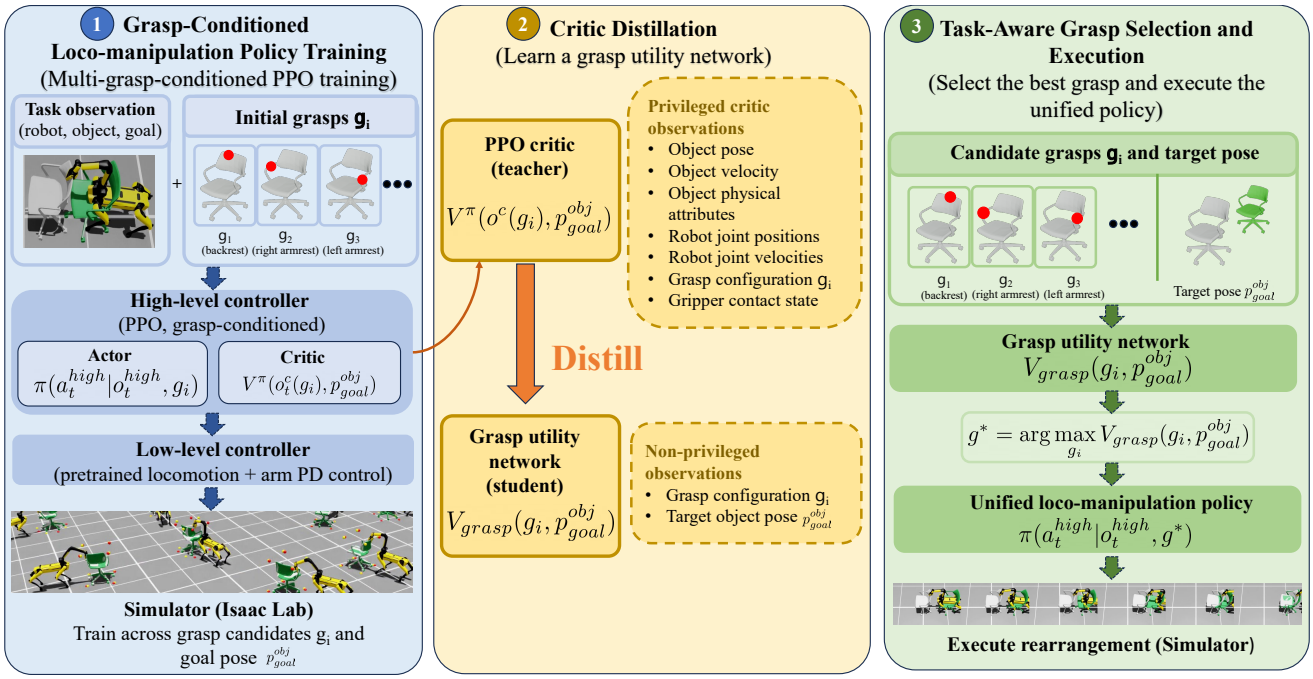


Fig. 3: **Overview of the proposed pipeline Grasp-TAGS.** (1) A hierarchical policy trained via PPO performs loco-manipulation using a pretrained low-level controller. (2) After PPO training, the learned critic is distilled into a grasp utility network. (3) At inference time, the distilled network selects the grasp g^* with the highest predicted downstream utility before policy execution.

learning efficiency, inspired by [9], [51], we adopt a hierarchical control architecture consisting of a pretrained low-level locomotion controller and a high-level task policy for manipulation. The low-level controller maintains locomotion stability, while the high-level policy generates task-related commands for object rearrangement. This decomposition allows the reinforcement learning agent to focus on task-level manipulation and planning without explicitly learning low-level locomotion dynamics (see Fig. 3)

1) Low-level controller: The low-level controller generates dynamically stable locomotion behaviors while tracking task-specific commands from the high-level controller. Specifically, the high-level command is defined as

$$a_t^{high} = (v_x^b, v_y^b, \omega_z^b, \Delta q_{arm,1:6}) \tag{4}$$

where v_x^b, v_y^b are the body linear velocities in the robot base frame, ω_z^b is the body yaw rate in the robot base frame, and $\Delta q_{arm,1:6}$ are the arm joint angle displacements. Inspired by [9], we execute the 6-dim arm commands directly with PD controllers, and we process base velocity commands with a pretrained locomotion policy into leg control commands to maintain stability. The locomotion policy receives the observation

$$o_t^{low} = (s_t^b, \dot{s}_t^b, \text{grav}_t, q_{1:18}, \dot{q}_{1:18}, a_t^{high}, a_{t-1}^{low}) \tag{5}$$

where $s_t^b \in \mathbb{R}^3$ denotes the observed body pose in robot base frame, $\dot{s}_t^b$ denotes the observed body velocity in robot base frame, $\text{grav}_t \in \mathbb{R}^3$ denotes the projected gravity vector, and $q_{1:18} = (q_{leg,1:12}, q_{arm,1:6}), \dot{q}_{1:18} = (\dot{q}_{leg,1:12}, \dot{q}_{arm,1:6}) \in \mathbb{R}^{18}$ denote the joint positions and velocities of all robot joints, including the leg joints and the arm joints. In addition, $a_t^{high} \in \mathbb{R}^9$ denotes the high-level command defined in Eq. 4. The locomotion policy produces 12-dimensional leg joint commands $a_t^{low} = q_{leg,1:12} \in \mathbb{R}^{12}$ which are executed by the robot to maintain locomotion stability and track the desired base velocity.

2) High-level controller: The high-level controller executes a policy focused on task-level planning and manipulation. Inspired by the observation terms in [7], Table II summarizes the observations o_t^{high} provided to the high-level controller. The high-level controller outputs the high-level command defined in Eq. 4, which the low-level controller then executes.

We train the high-level controller using Proximal Policy Optimization (PPO) [46], implemented in RSL-RLproposed [52], while keeping the pretrained low-level controller fixed throughout training. The objective is to maximize the expected discounted cumulative reward:

$$J(\pi_{high}^\theta, \pi_{low}) = \mathbb{E}_{r\sim p(\cdot|\pi_{high}^\theta, \pi_{low})}\left[\sum_{t=0}^{T-1} \gamma^t r_t\right] \tag{6}$$

where the reward r_t is composed of the terms described in Sec. IV-C. More training details can be found in Sec. IV-B

B. Grasp-Conditioned Loco-manipulation Policy Training

Rather than learning an independent high-level policy for each grasp, we train a grasp-conditioned policy via PPO [46] that operates across multiple initial grasp configurations, eliminating the need for separate training for each grasp on the same object [28]. Following [7], the arm joint angles implicitly encode the initial grasp pose.

TABLE I: Reward terms to train the high-level controller

Reward Terms	Formula	Weight	Description
Task completion	$\mathbb{1}[\{\|p_o - p_o^*\} < \varepsilon_p$	10.0	Positive reward when the object reaches the target pose
Keypoint pose matching	$\exp\left(-\frac{\|\mathbf{K}_{goal}-\mathbf{K}_{obj}\|_2}{\sigma^2}\right)$	8.0	Reduce the distance between the current and target object keypoints
Goal-directed velocity	$\exp\left(\frac{\hat{\mathbf{v}}_o \cdot \hat{\mathbf{d}}_{goal}}{\sigma^2} - 1\right)$	1.0	Encourage alignment between the object velocity and the direction toward the goal
Alive	$\mathbb{1}[episode\ is\ alive]$	5.0	Sparse reward for maintaining a valid and active episode
Linear velocity smoothness	$\|v_o\|^2$	-2.0	Penalty on changes in the object's linear velocity
Angular velocity smoothness	$\|\omega_o\|^2$	-2.0	Penalty on changes in the object's angular velocity
Orientation stability	$\mathbb{1}[\|g_{o,xy}\|^2 > \varepsilon_{orient}]$	-10.0	Encourage the object to maintain a desired upright/flat orientation
Joint configuration regularization	$\|q_{1:6} - q_{default,1:6}\|$	-5.0	Penalty based on the deviation of the robot joint positions from their default positions
Undesired contact penalty	$\mathbb{1}[\|F_{o,r}\| > \varepsilon_{contact}]$	-7.0	Penalty for undesired contacts during manipulation

TABLE II: Observation terms to the high-level controller. It consists of proprioceptive data from the robot and the real-time observations of the object.

Obs. Terms	Dim	Description
$q_{1:128}$	18	Position of all the joints (both arm & legs)
$\dot{q}_{1:128}$	18	Velocity of all the joints
s_t^b	2	Orientation of the base (no yaw)
$\dot{s}_t^b$	3	Angular velocity of the base
a_{t-1}^{high}	9	Last high-level action
$p_{ee,t}^b$	7	SE(3) pose of the end-effector in base frame
$p_{obj,t}^b$	3	SE(2) pose of the object in robot base frame
$p_{goal,t}^{obj}$	3	Target SE(2) pose in object frame

During training, each episode samples one of several predefined feasible grasp poses on the target object. After establishing the grasp, the robot is required to push or pull the object to a desired target pose (x,y,θ), where $x, y \in [-1, 1]$ and $\theta \in [-\frac{\pi}{2}, \frac{\pi}{2}]$. The policy therefore learns manipulation behaviors across different initial grasp configurations g_i and rearrangement objectives p_{goal}. We implement the training environment in IsaacLab [53] and train the high-level controller using PPO with 4096 parallel environments for 8000 iterations, as described in Sec. IV-A.2.

Training a unified policy across multiple grasp poses provides two key advantages. First, it enables the policy to capture the diverse interaction dynamics induced by different robot-object contact configurations without requiring separate training procedures for each grasp pose. Second, the resulting value function provides a common measure of the expected long-horizon manipulation performance across candidate grasp poses, which serves as the foundation for subsequent grasp pose selection (see Sec. VI).

C. Task-Specific Reward Functions

We design the reward function for the high-level controller according to three objectives: (i) *task completion*, which encourages the robot to transport the object to the desired pose; (ii) *motion smoothness*, which promotes smooth and non-aggressive manipulation behaviors; and (iii) *interaction stability*, which penalizes undesired robot-object contacts and object toppling. Table I summarizes the complete set of reward terms.

D. Critic Distillation for Task-Aware Grasp Selection

As illustrated in Fig. 3, the PPO critic [46] estimates the expected cumulative return from the current critic observation. Thus, the critic implicitly captures the expected downstream utility of different grasp configurations: grasps that enable more successful, efficient, and stable rearrangement should receive higher value estimates. At the beginning of an episode, different initial grasp poses $g_1, g_2, \ldots, g_K$ induce different critic observations $o^c(g_1), o^c(g_2), \ldots, o^c(g_K)$ at the start time $t = 0$. Together with the goal pose in the object frame p_{goal}^{obj}, the input to the critic can be represented as:

$$y_i = (o^c(g_i), p_{goal}^{obj}) \tag{7}$$

Consequently, the critic can provide different value estimates for the downstream task

$$V^\pi(y_i) = \mathbb{E}_\pi \left[\sum_{t=0}^{T-1} \gamma^t r_t \mid o^c(g_i), p_{goal}^{obj} \right]. \tag{8}$$

However, the critic relies on privileged information unavailable at inference time, including privileged physical and state information, such as object mass and velocity. Although these properties can potentially be estimated through physical interaction [7], [37], such interaction may require committing to an initial grasp. If that grasp is suboptimal, the robot must release and re-grasp the object, introducing additional manipulation steps and potential failure modes. We therefore avoid explicit physics estimation and instead distill the critic's grasp-dependent value into a lightweight grasp utility network $V_{\text{grasp}}(x_i)$ using only information on the candidate grasp and the goal object pose:

$$x_i = \left(g_i, p_{goal}^{obj}\right), \tag{9}$$

where g_i represents the candidate grasp configuration, and p_{goal}^{obj} is the target pose represented in the initial object frame, representing the task objective. By removing privileged physical variables from the input, the grasp selection network learns the expected grasp utility marginalized over the physical-property distribution encountered during training.

After policy training, we sample initial states from all N sub-environments and regress the utility network toward the

corresponding critic values:

$$\mathcal{L}_{\text{distill}} = \frac{1}{N}\sum_{k=1}^{N}\left[V_{grasp}(x_i^{(k)}) - V^{\pi}(y_i^{(k)})\right]^2. \quad (10)$$

where $g_i^{(k)}$ is the grasp candidate sampled in the k-th sub-environment, $x_i^{(k)}$ is the corresponding pre-interaction information and $y_i^{(k)}$ is the associated critic input as defined in Eq. 8

At inference, for the desired target object pose represented as p_{goal}^{obj}, we select

$$g^* = \arg\max_{g_i \in \mathcal{G}} V_{grasp}(x_i), \quad (11)$$

The manipulation policy is then executed conditioned on the selected grasp pose g^*

V. Experimental Setup

We evaluate the proposed grasp-pose-conditioned manipulation policy and critic-distilled grasp pose selection module on large-object rearrangement tasks through quantitative experiments in IsaacLab using synthetic object models.

A. Loco-manipulation Policy Evaluation in Simulation

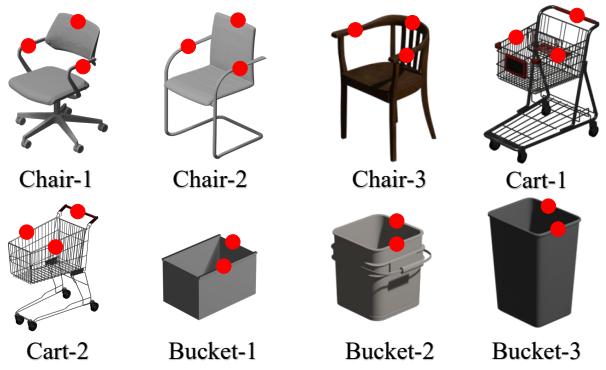


Fig. 4: **Objects and candidate grasp poses used in the experiments.** The dataset includes three chairs, two carts, and three buckets, with predefined candidate grasps highlighted in red. Candidate grasps used for our experiments are shown in red circle.

Dataset: We construct a dataset of eight common household large objects, including three chairs, two carts, and three buckets, obtained from Fab [54]. These objects represent common household object categories while covering diverse geometric structures, as shown in Fig. 4. For each object, we manually select feasible initial grasp configurations and compute their corresponding inverse kinematics solutions. Specifically:

- **Chairs:** three grasp poses on the two armrests and the backrest.
- **Carts:** three grasp poses on the two sides of the basket and the handle.
- **Buckets:** two grasp poses on the two edges.

Large Object Rearrangement Task: As described in Sec. III, we implement the large-object rearrangement task in IsaacLab [53]. At the beginning of each episode, the target object is placed at the origin and a target $SE(2)$ pose (x, y, θ) is randomly sampled, where $x, y \in [-1, 1]$ and $\theta \in [-\frac{\pi}{2}, \frac{\pi}{2}]$. For each object, we train one grasp-conditioned policy across all of its candidate grasps. We evaluate task performance using the metrics described below. We run all experiments in 4096 parallel environments.

Evaluation metrics: We evaluate the performance of the loco-manipulation policy under a given grasp pose using four metrics after a fixed execution horizon of 750 steps:

1) **Success rate:** the fraction of parallel sub-environments in which the final planar position error is below 0.1 m, and the final keypoint angular error is below 10° [17];
2) **Planar positional error**: measuring the final Euclidean distance on the xy-plane between the observed and target object positions;
3) **Angular error**: measuring the final absolute yaw difference between the observed and target object orientations.
4) **Keypoint Angular Error:** The angular difference between the observed and target object poses estimated from two sets of 2D object keypoints using the Kabsch–Umeyama alignment algorithm [55]. We use the eight corners of the object's bounding box as keypoints. This metric provides a more robust estimate of the orientation error than directly comparing the object yaw angles.

Baseline methods: We establish three baselines to evaluate the benefits of grasp-pose-conditioned policy learning and the proposed task-aware grasp pose selection module for large-object rearrangement. Specifically:

1) PPO_i**:** This baseline consists of policies trained exclusively on each grasp pose g_i (see Fig.4) using the same training procedure and hyperparameters. For example, PPO_1 is trained from scratch using only grasp pose g_1, without exposure to the other candidate grasp poses. These baselines evaluate the effect of training a policy across multiple grasp configurations.
2) PPO_g**+Random:** This baseline uses the proposed grasp-pose-conditioned loco-manipulation policy trained on all grasp candidates, but does not employ the grasp pose selection module. During both training and inference, a candidate grasp pose is randomly sampled at the beginning of each episode. This baseline isolates the contribution of task-aware grasp pose selection.
3) PPO_g**+Selection (Grasp-TAGS, Ours):** Our complete pipeline consists of the grasp-pose-conditioned loco-manipulation policy together with the critic-distilled grasp pose selection module. At inference time, the selection module evaluates the candidate grasp poses and selects the one with the highest predicted downstream task utility. This configuration represents the proposed method.

VI. Results

A. Loco-manipulation Policy Evaluation in Simulation

Our quantitative results indicate that the initial grasp configuration substantially affects downstream loco-manipulation performance (see Table III). Individually trained PPO_i policies can outperform PPO_g+Random

TABLE III: **Quantitative results on simulated large-object rearrangement.** We compare PPO_i, PPO_g+Random, and Grasp-TAGS using Success rate, Planar Positional Error, Angular Error and Keypoint Angular Error across multiple objects (↓: smaller numbers indicate better results; ↑: larger numbers indicate better results).

	Chair-1			**Chair2**		
	PPO_i	PPO_g **+ Random**	**Grasp-TAGS**	PPO_i	PPO_g **+ Random**	**Grasp-TAGS**
Success rate [%] (↑)	70.09/75.46/78.20	75.88	**93.65**	63.79/71.51/70.00	60.28	**84.72**
Planar Positional Error [m] (↓)	0.0292/0.0250/0.0366	0.0281	**0.0162**	0.034/**0.0161**/0.0142	0.045	0.0239
Angular Error [rad] (↓)	0.3571/0.2850/0.2802	0.2407	**0.0712**	0.5268/0.3421/0.3732	0.4382	**0.1308**
Keypoint Angular Error [deg] (↓)	20.4597/16.3271/16.0567	13.7906	**4.0793**	30.1858/19.5889/21.3821	25.1091	**7.4923**
	Chair-3			**Cart-1**		
	PPO_i	PPO_g **+ Random**	**Grasp-TAGS**	PPO_i	PPO_g **+ Random**	**Grasp-TAGS**
Success rate [%] (↑)	75.93/68.41/72.22	72.49	**89.62**	82.13/68.48/67.38	84.62	**95.51**
Planar Positional Error [m] (↓)	**0.0204**/0.0626/0.0307	0.041	0.0309	0.0291/0.0989/0.0924	0.0426	**0.0283**
Angular Error [rad] (↓)	0.3546/0.4425/0.3628	0.3616	**0.1212**	0.1716/0.2522/0.3781	0.1471	**0.0575**
Keypoint Angular Error [deg] (↓)	20.3148/25.3516/20.7884	20.7177	**6.9462**	9.8312/14.5265/20.9177	8.4009	**3.2925**
	Cart-2			**Bucket-1**		
	PPO_i	PPO_g **+ Random**	**Grasp-TAGS**	PPO_i	PPO_g **+ Random**	**Grasp-TAGS**
Success rate [%] (↑)	62.96/81.32/72.75	64.38	**86.89**	88.89/86.18	81.86	**92.58**
Planar Positional Error [m] (↓)	0.0901/**0.0235**/0.0762	0.1158	0.0551	**0.0101**/0.0280	0.0201	0.0138
Angular Error [rad] (↓)	0.4028/0.3335/0.3844	0.371	**0.1321**	0.1428/0.2250	0.2455	**0.1279**
Keypoint Angular Error [deg] (↓)	23.0807/19.1110/22.0228	21.2587	**7.5734**	8.1790/12.8935	14.0673	**7.3268**
	Bucket-2			**Bucket-3**		
	PPO_i	PPO_g **+ Random**	**Grasp-TAGS**	PPO_i	PPO_g **+ Random**	**Grasp-TAGS**
Success rate [%] (↑)	76.10/81.08	82.23	**91.87**	79.91/70.00	70.85	**83.89**
Planar Positional Error [m] (↓)	0.0219/0.0220	0.0144	**0.0105**	**0.0258** /0.0265	0.0689	0.029
Angular Error [rad] (↓)	0.3370/0.2490	0.2822	**0.1343**	0.2598/0.3199	0.3609	**0.2276**
Keypoint Angular Error [deg] (↓)	19.3076/14.2670	16.1711	**7.6976**	14.8877/18.3309	20.6764	**13.0426**

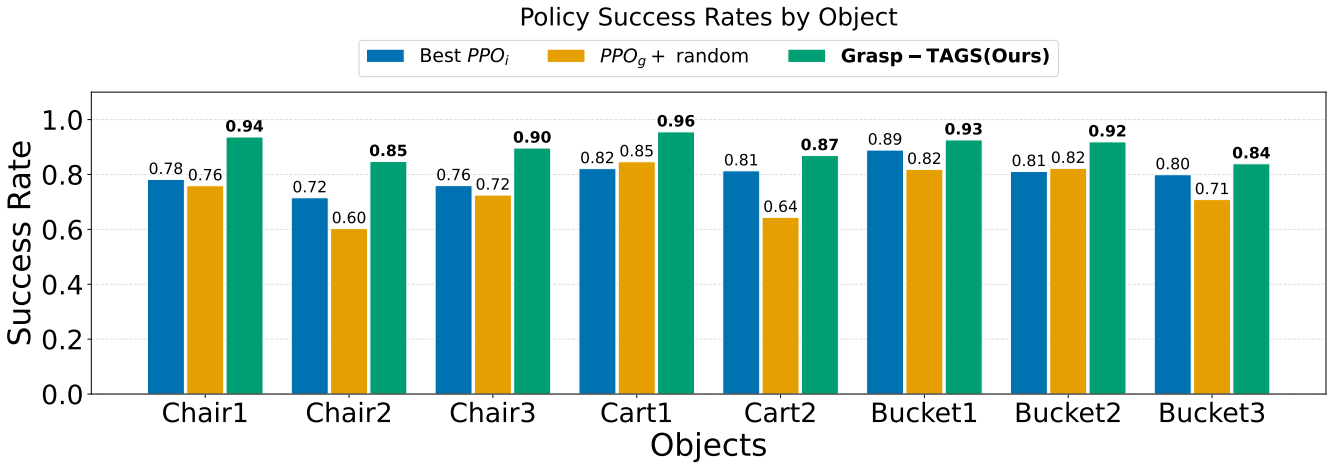


Fig. 5: **Success rates** for the best PPO_i among the policies trained individually on each grasp pose, PPO_g+random grasp selection, and Grasp-TAGS. Grasp-TAGS achieves the highest **success rate** (↑) across all evaluated objects in all 4096 parallel environments.

by achieving a higher success rate and lower positional or Angular Errors, because each policy specializes in a single robot-object interaction configuration. However, the relative performance of different grasps varies across rearrangement goals, motivating explicit task-aware grasp selection.

Combining the unified policy with the proposed grasp selection network improves average task success across all sub-environments (see Fig. 5). For Chair-1, Grasp-TAGS achieves a success rate of 93.65% over all sub-environments compared with 75.88% for random grasp selection and 69.02–78.20% for the individual single-grasp policies. The proposed method also achieves around a 60% lower Angular Error, suggesting that selecting an appropriate interaction configuration is particularly beneficial for tasks that require coordinated object translation and rotation. The same trend is observed for the other objects.

Quantitative Results: The quantitative results lead to the following observations:

1) **Success rate** (↑): Grasp-TAGS achieves the highest success rate across all eight evaluated objects. Compared with the best-performing single-grasp policy PPO_i, Grasp-TAGS improves success by 3.69–15.45 percentage points, and compared with PPO_g+Random, by 9.64–24.44 percentage points. Averaged across all objects, Grasp-TAGS achieves a success rate of 89.84%, compared with 79.87% for the best PPO_i baseline and 74.07% for PPO_g+Random. These results provide quantitative evidence that selecting the initial grasp according to predicted downstream task utility improves the reliability of large-object rearrangement.
2) **Planar Positional Error (↓):** Grasp-TAGS achieves the lowest planar positional error on Chair-1, Cart-1, and Bucket-2, and outperforms PPO_g+Random on all eight evaluated objects. On the remaining objects, the gap to



Fig. 6: **Illustrative example of grasp utility predictions for a target object pose (green mesh)**. The colors visualize the relative utility estimated by Grasp-TAGS, where green denotes higher predicted downstream utility and red denotes lower predicted utility.

the best single-grasp policy is small for Chair-2, Chair-3, Bucket-1, and Bucket-3, ranging from approximately 0.32 to 1.05 cm. The largest gap occurs on Cart-2, where Grasp-TAGS is 3.16 cm higher than the best PPO_i baseline. Averaged across all objects, Grasp-TAGS achieves a planar positional error of 2.60 cm, compared with 2.12 cm for the best single-grasp policies and 4.70 cm for PPO_g+Random.

3) Angular Error and Keypoint Angular Error: Grasp-TAGS achieves the lowest error under both orientation metrics across all eight evaluated objects. Compared with the strongest baseline for each object, the mean Angular Error decreases from 0.259 rad to 0.125 rad, corresponding to a reduction of approximately 51.6%. Similarly, the mean Keypoint Angular Error decreases from 14.82 to 7.18, a reduction of approximately 51.5%. These results indicate that task-aware grasp selection is particularly effective at improving final object orientation alignment with the desired target pose.
4) **Effect of Unified Policy Learning:** The single-grasp policies PPO_i often outperform PPO_g+Random because each policy specializes in a single grasp configuration, whereas the unified policy must accommodate a broader range of initial grasp conditions. Nevertheless, when combined with the proposed grasp selection module, the unified policy consistently achieves higher success rates than the best single-grasp baseline across all eight evaluated objects. On average, Grasp-TAGS improves the success rate from 79.87% for the best PPO_i baseline to 89.84%, corresponding to an absolute improvement of 9.97 percentage points. This result suggests that task-aware grasp selection can compensate for, and ultimately exceed, the performance advantage of individually specialized single-grasp policies.

These results suggest that grasp selection should consider downstream task utility rather than grasp stability alone [18]. In loco-manipulation, the initial grasp influences how effectively the robot controls the object throughout execution. Accordingly, our grasp selection network predicts the utility of candidate grasps and selects the most suitable one for the downstream task (Fig. 6), improving overall rearrangement performance. For more qualitative results, please refer to our webpage: `https://rpm-lab-umn.github.io/Grasp-TAGS-web-page/`

VII. Conclusion

We presented a task-aware grasp selection framework for prehensile goal-conditioned large-object loco-manipulation. By training one unified manipulation policy across multiple initial grasp configurations, the learned critic captures the long-horizon utility of different grasp configurations. Distilling these values into a lightweight grasp utility network enables the robot to select a suitable grasp before physical interaction without explicitly estimating privileged physical properties of the object. Simulation results demonstrate improved rearrangement success over fixed and randomly selected grasp configurations. Future work will extend the evaluation to additional household objects and real-world deployment on the SPOT platform.

Acknowledgement

The authors would like to thank Ebasa Temesgen for helps with the initial setup of Isaac Lab environment and all other members of the Robotics: Perception and Manipulation (RPM) Lab for their insightful discussions and proofreading of this paper.

References

[1] X. Tu and K. Desingh, "Superq-grasp: Superquadrics-based grasp pose estimation on larger objects for mobile-manipulation," in *2025 IEEE International Conference on Robotics and Automation (ICRA)*, 2025, pp. 3361–3368.

[2] Z. Fu, X. Cheng, and D. Pathak, "Deep whole-body control: Learning a unified policy for manipulation and locomotion," in *Conference on Robot Learning (CoRL)*, 2022.

[3] R. Mendonca, E. Panov, B. Bucher, J. Wang, and D. Pathak, "Continuously improving mobile manipulation with autonomous real-world rl," in *Conference on Robot Learning (CoRL)*, 2024.

[4] T. Li, J. Truong, J. Yang, A. Clegg, A. Rai, S. Ha, and X. Puig, "Robot-mover: Learning to move large objects from human demonstrations," *IEEE Transactions on Robotics*, 2026.

[5] J. Li and Q. Nguyen, "Multi-contact mpc for dynamic loco-manipulation on humanoid robots," *2023 American Control Conference (ACC)*, pp. 1215–1220, 2022. [Online]. Available: https://api.semanticscholar.org/CorpusID:252368129

[6] X. Wang, Y. Liu, X. Song, Y. Liu, S. Zhang, and S. Jiang, "An interactive navigation method with effect-oriented affordance," *2024 IEEE/CVF Conference on Computer Vision and Pattern Recognition (CVPR)*, pp. 16 446–16 456, 2024. [Online]. Available: https://api.semanticscholar.org/CorpusID:272723315

[7] Z. Bi, Y. Zhang, K. Chen, G. Zhao, Y. Li, and J. Ma, "Alore: Autonomous large-object rearrangement with a legged manipulator," *arXiv preprint arXiv:2602.04214*, 2026.

[8] Y. Ravan, Z. Yang, T. Chen, T. Lozano-P'erez, and L. P. Kaelbling, "Combining planning and diffusion for mobility with unknown dynamics," *arXiv preprint arXiv:2410.06911*, 2024.

[9] X. Zhu, Y. Chen, L. Sun, F. Niroui, S. L. Cleac'h, J. Wang, and K. Fang, "Versatile loco-manipulation through flexible interlimb coordination," in *9th Annual Conference on Robot Learning*, 2025. [Online]. Available: https://openreview.net/forum?id=Spg25qkV81

[10] C. Dai, X. Liu, K. Sreenath, Z. Li, and R. Hollis, "Interactive navigation with adaptive non-prehensile mobile manipulation," *IEEE Robotics and Automation Letters*, 2025.

[11] K. Ellis, H. Zhang, D. Stoyanov, and D. Kanoulas, "Navigation among movable obstacles with object localization using photorealistic simulation," 07 2022.

[12] M. Polverini, A. Laurenzi, E. Mingo Hoffman, F. Ruscelli, and N. Tsagarakis, "Multi-contact heavy object pushing with a centaur-type humanoid robot: Planning and control for a real demonstrator," *IEEE Robotics and Automation Letters*, vol. 5, pp. 859–866, 01 2020.

[13] Amazon FAR, P. Abbeel, J. Chen, R. Duan, A. Escontrela, M. Gandhi, S. Gundry, X. Huang, A. Kanazawa, T. Lewicki, J. Li, K. Liu, C. Rosenthal, Y. Seo, C. Sferrazza, G. Shi, L. Shih, J. Tseng, Z. Wu, L. Yang, B. Yi, and Y. Zhang, "Holosoma."

[14] C. Zheng, K. Chen, Z. Bi, Y. Li, L. Pan, J. Zhou, H. Li, and J. Ma, "Embracing bulky objects with humanoid robots: Whole-body manipulation with reinforcement learning," in *2026 IEEE International Conference on Robotics and Automation (ICRA)*, 2026.

[15] J. Z. Zhang, M. Sorokin, J. Brüdigam, B. Hung, S. Phillips, D. Yershov, F. Niroui, T. Zhao, L. Fermoselle, X. Zhu, C. Cao, D. Ta, T. Pang, J. Wang, P. Culbertson, Z. Manchester, and S. Le Cléac'h, "Sumo: Dynamic and generalizable whole-body loco-manipulation," *arXiv preprint arXiv:2604.08508*, 2026.

[16] C. Chi, S. Feng, Y. Du, Z. Xu, E. Cousineau, B. Burchfiel, and S. Song, "Diffusion policy: Visuomotor policy learning via action diffusion," in *Proceedings of Robotics: Science and Systems (RSS)*, 2023.

[17] I. Dadiotis, N. Tsagarakis, and M. Hutter, "Dynamic object goal pushing with mobile manipulators through model-free constrained reinforcement learning," 05 2025, pp. 13 363–13 369.

[18] A. Miller and P. Allen, "Graspit! a versatile simulator for robotic grasping," *IEEE Robotics and Automation Magazine*, vol. 11, no. 4, pp. 110–122, 2004.

[19] S. Kumra, S. Joshi, and F. Sahin, "Antipodal robotic grasping using generative residual convolutional neural network," in *2020 IEEE/RSJ International Conference on Intelligent Robots and Systems (IROS)*, 2020, pp. 9626–9633.

[20] M. A. Roa and R. Suárez, "Grasp quality measures: review and performance," *Auton. Robots*, vol. 38, no. 1, p. 65–88, Jan. 2015. [Online]. Available: https://doi.org/10.1007/s10514-014-9402-3

[21] H.-S. Fang, C. Wang, H. Fang, M. Gou, J. Liu, H. Yan, W. Liu, Y. Xie, and C. Lu, "Anygrasp: Robust and efficient grasp perception in spatial and temporal domains," *IEEE Transactions on Robotics (T-RO)*, 2023.

[22] M. Sundermeyer, A. Mousavian, R. Triebel, and D. Fox, "Contact-graspnet: Efficient 6-dof grasp generation in cluttered scenes," 2021.

[23] J. Mahler, M. Matl, X. Liu, A. Li, D. Gealy, and K. Goldberg, "Dex-net 3.0: Computing robust vacuum suction grasp targets in point clouds using a new analytic model and deep learning," in *2018 IEEE International Conference on Robotics and Automation (ICRA)*, 2018, pp. 1–8.

[24] M. B. Horowitz and J. W. Burdick, "Combined grasp and manipulation planning as a trajectory optimization problem," in *2012 IEEE International Conference on Robotics and Automation*, 2012, pp. 584–591.

[25] Z. Gao, J. Deng, Z. Wan, H. Zhang, Y. Wang, and J. Hu, "Grasp-clip: Pick up what you want," in *2025 IEEE International Conference on Industrial Technology (ICIT)*, 2025, pp. 1–6.

[26] H. Wang, Y. Wen, and Y. Zhang, "Tgdf: Task-oriented grasping through dense detection and foundation models," *Pattern Recognition Letters*, vol. 204, pp. 15–20, 2026. [Online]. Available: https://www.sciencedirect.com/science/article/pii/S0167865526001017

[27] F. Kaynar, S. Rajagopalan, S. Zhou, and E. Steinbach, "Remote task-oriented grasp area teaching by non-experts through interactive segmentation and few-shot learning," in *AAAI Workshop on Artificial Intelligence for User-Centric Assistance for at Home Tasks*, Feb. 2023.

[28] L. Röstel, D. Winkelbauer, L. Pitz, Johannes Sievers, and B. Bäuml, "Composing dextrous grasping and in-hand manipulation via scoring with a reinforcement learning critic," in *2025 IEEE International Conference on Robotics and Automation (ICRA)*. IEEE, May 2025.

[29] K. Black, N. Brown, J. Darpinian, K. Dhabalia, D. Driess, A. Esmail, M. R. Equi, C. Finn, N. Fusai, M. Y. Galliker, D. Ghosh, L. Groom, K. Hausman, b. ichter, S. Jakubczak, T. Jones, L. Ke, D. LeBlanc, S. Levine, A. Li-Bell, M. Mothukuri, S. Nair, K. Pertsch, A. Z. Ren, L. X. Shi, L. Smith, J. T. Springenberg, K. Stachowicz, J. Tanner, Q. Vuong, H. Walke, A. Walling, H. Wang, L. Yu, and U. Zhilinsky, "$\pi_{0.5}$: a vision-language-action model with open-world generalization," in *Proceedings of The 9th Conference on Robot Learning*, ser. Proceedings of Machine Learning Research, J. Lim, S. Song, and H.-W. Park, Eds., vol. 305. PMLR, Sep. 2025, pp. 17–40. [Online]. Available: https://proceedings.mlr.press/v305/black25a.html

[30] K. Black, N. Brown, D. Driess, A. Esmail, M. R. Equi, C. Finn, N. Fusai, L. Groom, K. Hausman, B. Ichter, S. Jakubczak, T. Jones, L. Ke, S. Levine, A. Li-Bell, M. Mothukuri, S. Nair, K. Pertsch, L. X. Shi, L. Smith, J. Tanner, Q. Vuong, A. Walling, H. Wang, and U. Zhilinsky, "π_0: A vision-language-action flow model for general robot control," in *Proceedings of Robotics: Science and Systems*, Los Angeles, CA, USA, Jun. 2025.

[31] A. Brohan, N. Brown, J. Carbajal, Y. Chebotar, J. Dabis, C. Finn, K. Gopalakrishnan, K. Hausman, A. Herzog, J. Hsu, J. Ibarz, B. Ichter, A. Irpan, T. Jackson, S. Jesmonth, N. J. Joshi, R. Julian, D. Kalashnikov, Y. Kuang, I. Leal, K.-H. Lee, S. Levine, Y. Lu, U. Malla, D. Manjunath, I. Mordatch, O. Nachum, C. Parada, J. Peralta, E. Perez, K. Pertsch, J. Quiambao, K. Rao, M. S. Ryoo, G. Salazar, P. R. Sanketi, K. Sayed, J. Singh, S. Sontakke, A. Stone, C. Tan, H. Tran, V. Vanhoucke, S. Vega, Q. Vuong, F. Xia, T. Xiao, P. Xu, S. Xu, T. Yu, and B. Zitkovich, "Rt-1: Robotics transformer for real-world control at scale," in *Proceedings of Robotics: Science and Systems*, Daegu, Republic of Korea, Jul. 2023.

[32] B. Zitkovich, T. Yu, S. Xu, P. Xu, T. Xiao, F. Xia, J. Wu, P. Wohlhart, S. Welker, A. Wahid, Q. Vuong, V. Vanhoucke, H. Tran, R. Soricut, A. Singh, J. Singh, P. Sermanet, P. R. Sanketi, G. Salazar, M. S. Ryoo, K. Reymann, K. Rao, K. Pertsch, I. Mordatch, H. Michalewski, Y. Lu, S. Levine, L. Lee, T.-W. E. Lee, I. Leal, Y. Kuang, D. Kalashnikov, R. Julian, N. J. Joshi, A. Irpan, B. Ichter, J. Hsu, A. Herzog, K. Hausman, K. Gopalakrishnan, C. Fu, P. Florence, C. Finn, K. A. Dubey, D. Driess, T. Ding, K. M. Choromanski, X. Chen, Y. Chebotar, J. Carbajal, N. Brown, A. Brohan, M. G. Arenas, and K. Han, "Rt-2: Vision-language-action models transfer web knowledge to robotic control," in *Proceedings of the 7th Conference on Robot Learning*, ser. Proceedings of Machine Learning Research, vol. 229. PMLR, 2023, pp. 2165–2183.

[33] Octo Model Team, D. Ghosh, H. Walke, K. Pertsch, K. Black, O. Mees, S. Dasari, J. Hejna, C. Xu, J. Luo, T. Kreiman, Y. Tan, L. Y. Chen, P. Sanketi, Q. Vuong, T. Xiao, D. Sadigh, C. Finn, and S. Levine, "Octo: An open-source generalist robot policy," in *Proceedings of Robotics: Science and Systems*, Delft, Netherlands, 2024.

[34] M. J. Kim, K. Pertsch, S. Karamcheti, T. Xiao, A. Balakrishna, S. Nair, R. Rafailov, E. P. Foster, P. R. Sanketi, Q. Vuong, T. Kollar, B. Burchfiel, R. Tedrake, D. Sadigh, S. Levine, P. Liang, and C. Finn, "Openvla: An open-source vision-language-action model," in *Proceedings of the 8th Conference on Robot Learning*, ser. Proceedings of Machine Learning Research, vol. 270. PMLR, 2024, pp. 2679–2713.

[35] T. Z. Zhao, V. Kumar, S. Levine, and C. Finn, "Learning fine-grained bimanual manipulation with low-cost hardware," in *Proceedings of Robotics: Science and Systems*, Daegu, Republic of Korea, Jul. 2023.

[36] Z. Bing, Y. Yun, K. Huang, and A. Knoll, "Context-based meta-reinforcement learning with bayesian nonparametric models," *IEEE Transactions on Pattern Analysis and Machine Intelligence*, vol. 46, no. 10, pp. 6948–6965, 2024.

[37] M. Wang, S. Tian, A. Swann, O. Shorinwa, J. Wu, and M. Schwager, "Phys2real: Fusing vlm priors with interactive online adaptation for uncertainty-aware sim-to-real manipulation," in *IEEE International Conference on Robotics and Automation (ICRA)*, 2026.

[38] A. Shankar, J. Blumenkamp, and A. Prorok, "Language-conditioned offline rl for multi-robot navigation," 05 2025, pp. 14 984–14 991.

[39] F. Ye, Y. Lin, Y. Lai, and Q. Huang, "Task-oriented language grounding for robot via learning object mask," in *2024 6th International Conference on Robotics, Intelligent Control and Artificial Intelligence (RICAI)*, 2024, pp. 16–22.

[40] J. Hu, R. Hendrix, A. Farhadi, A. Kembhavi, R. Martín-Martín, P. Stone, K.-H. Zeng, and K. Ehsani, "Flare: Achieving masterful and adaptive robot policies with large-scale reinforcement learning fine-tuning," in *2025 IEEE International Conference on Robotics and Automation (ICRA)*, 2025, pp. 3617–3624.

[41] M. Nakamoto, O. Mees, A. Kumar, and S. Levine, "Steering your generalists: Improving robotic foundation models via value guidance," *Conference on Robot Learning (CoRL)*, 2024.

[42] T. Schaul, D. Horgan, K. Gregor, and D. Silver, "Universal value function approximators," in *Proceedings of the 32nd International Conference on Machine Learning*, ser. Proceedings of Machine Learning Research, F. Bach and D. Blei, Eds., vol. 37. Lille, France: PMLR, Jul. 2015, pp. 1312–1320. [Online]. Available: https://proceedings.mlr.press/v37/schaul15.html

[43] M. Andrychowicz, F. Wolski, A. Ray, J. Schneider, R. Fong, P. Welinder, B. McGrew, J. Tobin, P. Abbeel, and W. Zaremba, "Hindsight experience replay," in *Proceedings of the 31st International Conference*

on Neural Information Processing Systems, ser. NIPS'17. Red Hook, NY, USA: Curran Associates Inc., 2017, p. 5055–5065.

[44] X. Feng, "Multi-goal reinforcement learning via exploring successor matching," in *2022 IEEE Conference on Games (CoG)*, 2022, pp. 401–408.

[45] Y. W. Teh, V. Bapst, W. M. Czarnecki, J. Quan, J. Kirkpatrick, R. Hadsell, N. Heess, and R. Pascanu, "Distral: robust multitask reinforcement learning," in *Proceedings of the 31st International Conference on Neural Information Processing Systems*, ser. NIPS'17. Red Hook, NY, USA: Curran Associates Inc., 2017, p. 4499–4509.

[46] J. Schulman, F. Wolski, P. Dhariwal, A. Radford, and O. Klimov, "Proximal policy optimization algorithms," *arXiv preprint arXiv:1707.06347*, 2017.

[47] E. Xiang, H. Ma, X. Ma, Z. Liu, and D. Huang, "Graspldp: Towards generalizable grasping policy via latent diffusion," in *Proceedings of the IEEE/CVF Conference on Computer Vision and Pattern Recognition (CVPR)*, Jun. 2026, pp. 28 032–28 041.

[48] B. Hu, H. Tian, D. Wang, H. Huang, X. Zhu, R. Walters, and R. Platt, "Push-grasp policy learning using equivariant models and grasp score optimization," *IEEE Robotics and Automation Letters*, 2025.

[49] E. Foong, Y. Li, H. Jiang, G. S. Sukhatme, and D. Seita, "Handful: Sequential grasp-conditioned dexterous manipulation with resource awareness," in *2026 IEEE/RSJ International Conference on Intelligent Robots and Systems (IROS)*, 2026.

[50] K. Fang, Y. Zhu, A. Garg, A. Kuryenkov, V. Mehta, L. Fei-Fei, and S. Savarese, "Learning task-oriented grasping for tool manipulation from simulated self-supervision," *Robotics: Science and Systems (RSS)*, 2018.

[51] A. Kumar, Z. Fu, D. Pathak, and J. Malik, "RMA: Rapid motor adaptation for legged robots," *Robotics: Science and Systems*, 2021.

[52] C. Schwarke, M. Mittal, N. Rudin, D. Hoeller, and M. Hutter, "Rsl-rl: A learning library for robotics research," *arXiv preprint arXiv:2509.10771*, 2025.

[53] M. Mittal, P. Roth, J. Tigue, A. Richard, O. Zhang, P. Du, A. Serrano-Muñoz, X. Yao, R. Zurbrügg, N. Rudin, L. Wawrzyniak, M. Rakhsha, A. Denzler, E. Heiden, A. Borovicka, O. Ahmed, I. Akinola, A. Anwar, M. T. Carlson, J. Y. Feng, A. Garg, R. Gasoto, L. Gulich, Y. Guo, M. Gussert, A. Hansen, M. Kulkarni, C. Li, W. Liu, V. Makoviychuk, G. Malczyk, H. Mazhar, M. Moghani, A. Murali, M. Noseworthy, A. Poddubny, N. Ratliff, W. Rehberg, C. Schwarke, R. Singh, J. L. Smith, B. Tang, R. Thaker, M. Trepte, K. V. Wyk, F. Yu, A. Millane, V. Ramasamy, R. Steiner, S. Subramanian, C. Volk, C. Chen, N. Jawale, A. V. Kuruttukulam, M. A. Lin, A. Mandlekar, K. Patzwaldt, J. Welsh, H. Zhao, F. Anes, J.-F. Lafleche, N. Moënne-Loccoz, S. Park, R. Stepinski, D. V. Gelder, C. Amevor, J. Carius, J. Chang, A. H. Chen, P. de Heras Ciechomski, G. Daviet, M. Mohajerani, J. von Muralt, V. Reutskyy, M. Sauter, S. Schirm, E. L. Shi, P. Terdiman, K. Vilella, T. Widmer, G. Yeoman, T. Chen, S. Grizan, C. Li, L. Li, C. Smith, R. Wiltz, K. Alexis, Y. Chang, D. Chu, L. J. Fan, F. Farshidian, A. Handa, S. Huang, M. Hutter, Y. Narang, S. Pouya, S. Sheng, Y. Zhu, M. Macklin, A. Moravanszky, P. Reist, Y. Guo, D. Hoeller, and G. State, "Isaac lab: A gpu-accelerated simulation framework for multi-modal robot learning," *arXiv preprint arXiv:2511.04831*, 2025.

[54] Epic Games, Inc., "Fab," https://www.fab.com/, 2026, 3D asset marketplace.

[55] S. Umeyama, "Least-squares estimation of transformation parameters between two point patterns," *IEEE Transactions on Pattern Analysis and Machine Intelligence*, vol. 13, no. 4, pp. 376–380, 1991.